# Simple analytical embedded-atom-potential model including a long-range force for fcc metals and their alloys

J. Cai
*Department of Physics, Wuhan University, Wuhan 430072, People's Republic of China*

Y. Y. Ye
*Centre of Instrumental Analysis, Wuhan University, Wuhan 430072, China*

(Received 19 October 1995; revised manuscript received 4 March 1996)

A simple analytical embedded-atom method (EAM) model is developed. The model includes a long-range force. In this model, the electron-density function is taken as a decreasing exponential function, the two-body potential is defined as a function like a form given by Rose *et al.* [Phys. Rev. B **33**, 7983 (1986)], and the embedding energy is assumed to be an universal form recently suggested by Banerjea and Smith. The embedding energy has a positive curvature. The model is applied to seven fcc metals (Al, Ag, Au, Cu, Ni, Pd, and Pt) and their binary alloys. All the considered properties, whether for pure metal systems or for alloy systems, are predicted to be satisfactory at least qualitatively. The model resolves the problems of Johnson's model for predicting the properties of the alloys involving metal Pd. However, more importantly, (i) by investigating the structure stability of seven fcc metals using the present model, we found that the stability energy is dominated by both the embedding energy and the pair potential for fcc-bcc stability while the pair potential dominates and is underestimated for fcc-hcp stability; and (ii) we find that the predicted total energy as a function of lattice parameter is in good agreement with the equation of state of Rose *et al.* for all seven fcc metals, and that this agreement is closely related to the electron density, i.e., the lower the contribution from atoms of the second-nearest neighbor to host density, the better the agreement becomes. We conclude the following: (i) for an EAM, where angle force is not considered, the long-range force is necessary for a prediction of the structure stability; or (ii) the dependence of the electron density on angle should be considered so as to improve the structure-stability energy. The conclusions are valid for all EAM models where an angle force is not considered. [S0163-1829(96)07727-2]

## I. INTRODUCTION

Pair potentials have until now been the most popular approach for calculating bulk and defect properties of solids. However, a pair-potential model does not represent the free-electron energy in real metals, which is of considerable importance in calculations for various problems, such as vacancy formation energy and elastic constants; also, the ambiguity of volume concerning a defect is not avoided in the pair potentials.[1,2] On the other hand, although self-consistent energy-band and total-energy calculations using the density-functional formalism[3] have shown exactitude for treating such problems, using them to perform calculations for a system containing a large number of particles is not a practical proposal at the moment. Hence developing an empirical (or semiempirical) method which can solve these problems of a pair potential, but which is more efficient than the first-principles technique, is of great interest. In the last ten years, this technique for treating metal systems (even for treating covalent materials[4]) has been developed and used successfully in quite extensive fields of computer simulation involving material science.[1,2,4,5,7–13] This method was originally presented by Daw and Baskes,[1] and its basic ideal can be interpreted in the framework of density-functional theory.[3] From the point of view of this theory, the energy required to place a small impurity atom in a lattice is determined solely by the electron density at that particular site, without considering the origin of the electron density.[3] A significant contribution of Daw and Baskes is that they extended this ideal to write the energy as an embedding energy plus a core-core repulsion potential. This embedding energy and repulsion potential can then be obtained by fitting experimental data. Though this method is found to be simple, it can correctly represent the structure and energetics of more flexible metal systems, such as surface, defects, impurities *et al.*[1] This method is called the embedded-atom method (EAM). Subsequently, various similar models were also proposed by many authors.[2,4,5,7–12]

In the development of this method, as seen, an underlying theme is computational simplicity, so that the interactions may readily be used for large molecular dynamics or Monte Carlo simulations. The EAM of Daw and Baskes is simple, but its embedded energy and pair potential are given in the form of spline functions.[1] Indeed, this will give rise to some inconvenience for calculations. More unfortunately, due to its unanalytical form this EAM model is not easy to use to make an extension including an angle force, while a more flexible EAM model should include an angle force.[4] Likewise, the initial EAM of Daw and Baskes cannot be used to study alloys, since the information used in Daw and Baskes' empirical fit actually only determines the embedding energy and its first two derivatives for electron densities near the average host electron density of the bulk pure materials at equilibrium.[5] Foiles, Bakes, and Daw gave another modified version, where the total energy of a system is designed to follow the equation of state of Rose *et al.*,[6] and the pair

 

potential is assumed to be an analytical form. The embedding energy can be determined by this total energy minus the energy of the pair potential, and becomes a tabulate function of the host electron density.[5] Thus properties away from the equilibrium state are regarded as fitted in this method. Following this ideal, many authors also constructed various specified potential models.[7–10] Johnson's analytical nearest-neighbor model[7] is, more or less, inspired by this ideal. But, the weakness of this scheme is that the second derivative of the embedding energy will become smaller than zero in the case when the two-body potential changes more rapidly than the equation of state of Rose *et al.* This behavior may give an incorrect coordination dependence between bond length and energy,[13] and is not observed in the calculations of effective-medium or quasiatom theory.[14–16] In addition, as in the initial EAM of Daw and Baskes, this method may be difficult to extend to include an angle force due to the unanalytical form of the embedding energy. Though Johnson gave an analytical EAM model[7,9] which is similar to Foiles, Baskes, and Daw's model, Johnson's model suffers from some problems of dilute-limit heats of the solution and the phase stability of alloy systems involving metal palladium.[8,9] In the present paper we will present an alternative completely analytical EAM model which includes a long-range force. In this model, the electron-density function is taken as an exponentially decreasing function, the two-body potential is defined as a function like a form given by Rose *et al.*[6] and the embedding energy is assumed to be of the universal form recently suggested by Banerjea and Smith.[17] The potential parameters of this model are determined by fitting the basic bulk properties of a pure metal. This development is important because (i) its embedded energy has a positive curvature and this potential resolves the problem of Johnson's potential model mentioned above; (ii) its simple and analytical form may be easy to use to make a further extension including an angle force; and (iii) this model can reproduce the equation of state of Rose *et al.*[6] very well (see below), and this point is necessary for calculating the properties of a system, say an alloy system, where the host electron density is well away from that of bulk pure material at equilibrium. To our knowledge, our present model is the simplest one in its form. One of our purposes is to present a simpler and more practicable EAM model.

In order to test the reliability of our present model, the model is applied to seven fcc metals (Al, Ag, Au, Cu, Ni, Pd, and Pt) and all their binary alloys. The properties, including the equation of state, surface relaxation, surface energy, divacancy binding energy, and the formation energy of vacancy at (111) surfaces of the seven pure metals, as well as the dilute-limit heats of solution of the alloys, the heats of formation, and the lattice constants of the intermetallic compounds with $L1_2$ and $L1_0$ structures, are calculated. All the results predicted, whether for pure metals or their alloys, are found to be in agreement with those from experiments or from more level calculations expected for only one case of impurity Pd in host Ni. Moreover, in order to understand the limit of an EAM model, we investigate the structure stability and equation of state and discuss their physical origins. These will show that (i) for an EAM, where angle force is not considered, the long-range force is necessary for a prediction of the structure stability; and (ii) the dependence of the electron density on angle should be considered so as to improve the structure-stability energy.

This paper is arranged as follows: First, we give our potential model. Then we present some applications of the model to the seven pure metals and their alloys, and the structure stability and equation of state are also discussed in detail. Finally, we summarize our main conclusions.

## II. MODEL AND METHOD

Within the framework of the EAM theory, the total internal energy of the system of $N$ atoms is described as the energy required to embed these $N$ atoms into the homogeneous electron gas caused by surrounding atoms plus a correction of energy from two-body interactions. Thus this total energy can be expressed as [1]

$$E_{\rm tot}=\sum_i F_i(\rho_i)+\sum_{i>j}\phi(r_{ij}), \tag{1}$$

where $E_{\rm tot}$ is the total internal energy, $F_i(\rho_i)$ is the embedding energy required to place atom $i$ in an electron density $\rho_i$, $\phi(r_{ij})$ is the two-body potential between atoms $i$ and $j$, $r_{ij}$ is the separation distance related to the specified pair of atoms $i$ and $j$, and $\rho_i$ denotes the host electron density at atom $i$ due to all other atoms. According to the linear superposition approximation this host electron density can be written as the sum of the electron density $f(r_{ji})$ of the individual atom $j$, i.e.,

$$\rho_i=\sum_{j(\neq i)} f(r_{ji}). \tag{2}$$

Note that the embedding function $F(\rho)$ is universal, in that it does not depend on the source of the host electron density. Thus the same embedding function can be used principally to calculate the energy of an atom in an alloy that is used in the pure material. However a trap should be avoided; i.e., in this situation the embedding energy must be determined in a wide range of host electron density rather than only at equilibrium. Foiles, Baskes, and Daw[5] have shown that this can be accomplished by requiring that the total energy as a function of lattice parameter follows the equation of state of Rose *et al.*[6] We will show that it can also be attained by virtue of an alternative method below.

As seen above, Eq. (1) has a clearcut physical picture, but based on different underlying theories it can be interpreted in different manners.[2,11] This makes $F(\rho)$, $\phi(r)$, and $f(r)$ able to take different specific functional forms, respectively. Finnis and Sinclair proposed that the $d$-$d$ hybridization in the second-moment approximation can be described by Eq. (1). This ''$N$-body'' potential has been applied to defects in bcc metals.[2] The ''local volume forces'' represents an alternative parametrization of the EAM by Voter and Chen, and has been applied to surface relaxation and grain boundaries in binary metallic alloys.[10] The ''glue model'' of Ercolessi, Tosatti, and Parrinello also belongs to the EAM class of models, and has been applied mainly to surface reconstructions.[11] The embedding function and pair interaction can also be obtained from first-principles calculations.[18,19] In practice, one prefers an empirical or semiempirical approach to obtain these functions. In many earlier

EAM models,[5,10] $\phi$ is assumed to be an analytical form, and $F(\rho)$ is a tabulated function of the host electron density. More recently Johnson gives an analytic EAM model for fcc metals.[7] The deficiencies of these models were mentioned in Sec. I, and we do not attempt to repeat it here. In our present scheme, we have fixed analytical forms of $\phi(r)$, $F(\rho)$, and $f(r)$, chosen to be physically plausible, and adjusted so that they would well reproduce basic physical properties of a pure metal.

Banerjea and Smith have shown that a simple exponential function can be used to represent the host electron density quite well for bulk, near-vacancies, and free surfaces, and for diatomics.[17] Thus, at the approximation level, we can assume that the atomic electron density also follows this exponential form, and we obtain

$$f(r)=f_e\exp[-\chi(r-r_e)], \tag{3}$$

where $f_e$ is a scaling constant, $r_e$ is the equilibrium nearest distance, and $\chi$ is an adjustable parameter that must be determined. In obtaining additional functions of the EAM, a caution should be kept in mind; that is, the embedding function should have positive curvature. This ensures that the bond strength decreases with increasing coordination.[13] In our model we take the embedding function as the universal form suggested by Banerjea and Smith;[17] then

$$F(\rho)=-F_0\left[1-\ln\left(\frac{\rho}{\rho_e}\right)^n\right]\left(\frac{\rho}{\rho_e}\right)^n+F_1\left(\frac{\rho}{\rho_e}\right). \tag{4}$$

Note that we add a linear term [the second term on the left in Eq. (4)] to the original formula of Benerjea and Smith.[17] This treatment does not destroy its positive definition curvature. Benerjea and Smith pointed out[17] that a decreasing exponential curvature function combining with the universal embedding function may yield the model function of Rose *et al.*[6] We expect that the sum of two model functions similar to that of Rose *et al.* also give the invariant form (or at least an approximate form) of the Rose *et al.* model function. Thus in our EAM model we define the two-body potential as an analytical form like the Rose *et al.* model function. We have

$$\phi(r)=-\alpha[1+\beta(r/r_a-1)]\exp[-\beta(r/r_a-1)]. \tag{5}$$

Below we will see that the above functions can reproduce the equation of Rose *et al.* very well (this is not guaranteed by the fitting). Thus we believe that we obtain a set of functions for the EAM which can well describe the properties away from equilibrium. Though the method of Foiles, Baskes, and Daw[5] also gives a set of functions for the EAM, in this method the embedding energy will be negatively defined as the two-body potential changes more rapidly than the equation of state of Rose *et al.* We now turn back. In Eqs. (4) and (5), $\rho_e$ represents the host electron density at equilibrium, and $F_0$ and $n$ are two constants. We take $F_0=E_c-E_v^f$, and $n=0.5$, where $E_c$ and $E_v^f$ are the cohesive energy and vacancy formation energy, respectively. We do this without any physical consideration and only for convenience. The remainder—$r_a$, $F_1$, $\alpha$, and $\beta$—plus another parameter $\chi$ appearing in Eq. (3) make up five parameters that must be determined for pure element systems. $f_e$ is a scaling factor, and cancels from the model for the pure element system because only ratios of electron densities occur in Eq. (5). Without a loss in general, for pure metals the $f_e$ can be taken as unit. But for an alloy system the scaling factor $f_e$ should be specified by the properties of the alloy. Details will be given in Sec. III.

Having specified the functional forms of $f(r)$, $\phi(r)$, and $F(\rho)$, we now describe the fitting procedure. The parameters $\chi$, $\alpha$, $\beta$, $r_a$, and $F_1$ are determined by minimizing the root-square deviation ($X_{\rm rmx}$) between calculated and experimental thermodynamic data. This is accomplished using a simplex procedure.[20] For the materials Al, Ag, Au, Cu, Ni, Pd, and Pt the experimental data consist of the three elastic constants ($C_{11}$, $C_{12}$, and $C_{44}$), the vacancy formation energy ($E_v^f$), the equilibrium lattice constant ($a_0$), and the cohesive energy ($E_c$). In fitting we take the cutoff distance as $r_{\rm cut}=1.65a_0$. The fitting results and the potential parameters, together with the experimental data to which they were fitted, are displayed in Table I. As seen in Table I, the calculated lattice constants and the vacancy formation energies are in excellent agreement with the respective experimental data, expect for the vacancy formation energy of Ni, with an error of 0.03 eV. For cohesive energies the agreement of the prediction and experiment is also seen to be good, and the largest difference is 0.05 eV between the prediction and the experiment. The calculated elastic constants are in general agreement with experimental results, though for Ni the difference of $C_{12}$ between the predicted and experimental results remains as large as 21%.

For a comparison, it is worth mentioning that in the model of Foiles, Baskes, and Daw the largest difference between the predicted and the experimental results are found to be equal to 0.18 eV and 20% for vacancy formation and elastic constants, respectively, though the cohesive energy and the lattice constant are identical to the respective experimental values.[5] Thus our model can predict the vacancy formation energy better than that of Foiles, Baskes, and Daw, and the elastic constants as good as those of Ref. 5.

Figures 1(a) and 1(b) show our resulting functions of the $\phi(r)$ and the $F(\rho)$ of the seven metals. From the figures we can see that the two-body potentials include long-range interactions, and the general characters of the shapes of the embedding energies from the present model are identical to those from first-principles calculation;[14–16] that is, a minimum is seen in the embedding energies, and then the embedding energies rise monotonically with the host electron density. In other words, the embedding energies have a positive curvature in the present potential model. The positive curvature of the embedding function determined by the scheme of Ref. 5 cannot be always maintained, because it will become negatively defined for the case in which the two-body potential changes more rapidly than the equation of state of Rose *et al.*

Baskes[4] extended an analytical nearest-neighbor EAM model to include directional bonding (angle force), where the two-body potential is obtained from an inversion of total energy minus embedding energy which is assumed to be an analytical form in advance. This modified EAM is complex even for the simplification of first-neighbor interactions. As is well known, a long-range force is important for treating the problems involving long-range correlation. If we make an extension of the modified EAM to include a long-range force, the process will become more complex. Our present

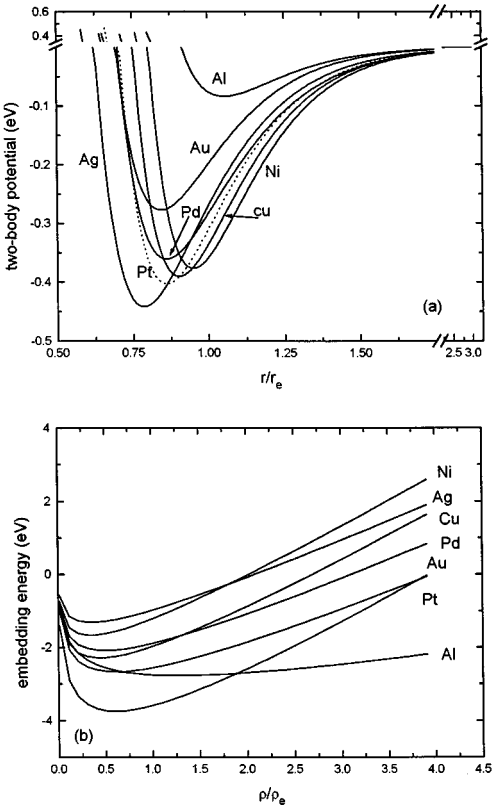


FIG. 1. (a) Two-body potential and (b) embedding energy.

EAM model is simple, and includes the long-range force. This model should be easier to extend, including an angle force where the two-body potential is obtained by an inversion method similar to that of Baskes. We will make this extension in a sequel to this paper.

## III. APPLICATION TO BULKS, DEFECTS, SURFACES, AND ALLOYS

Generally, in computer simulations, the potential function and its first derivatives with respect to atomic coordinates should be continuous at all geometries of the system. This can be accomplished by forcing the atomic electron density $f(r)$ and pair potential $\phi(r)$ and their first derivatives $f(r)'$ and $\phi(r)'$ to go smoothly to zero at a cutoff distance using a cutoff function. However, in our present model we consider only a long-range interaction, instead of any cutoff procedure. We find that when we take a cutoff distance of $r_{\rm cut}=1.65a_0$, which lays between the fifth and the sixth neighbors, the ratio of energy from the fifth neighbor to the total internal energy are all consistently less than 0.05% for all seven metals. Thus we believe that the potential goes smoothly to zero within the error of 0.05%.

### A. Structure stability and equation of state

In the present EAM model, the fitting is not artificially constrained by the requirement that the fcc crystal structure be more stable than a bcc and a hcp with an ideal $c/a$ ratio, in which the bcc or hcp have the same atomic volume in magnitude as the fcc does. However, as known, the global stability is very important, and will guarantee that any small perturbations will not lead to a spontaneous transformation to a different lattice structure. Therefore, calculation of the cohesive energies of each structure can provide an important information to test the reliability of the potential. We will calculate the cohesive energies of the fcc, bcc, and hcp for all seven metals Al, Ag, Au, Cu, Ni, Pd, and Pt with a cutoff distance of $r_{\rm cut}=1.65a_0$. The calculated results, together with the results derived from the experimental stacking fault or phase diagram information (see Table VI in Ref. 4), are listed in Table II. From the table we see that the calculated energies of fcc-hcp stability (the difference of cohesive energies between two dissimilar structures) are generally less than as much as one order of magnitude of the experimental value, and the calculated energy of the fcc-bcc stability is equal to about a factor of 2 of the corresponding experimental value in magnitude. However, from the calculations it can be obtained that the fcc structures have the largest cohesive energy, that the hcp mediates, and that the bcc is the lowest for all seven metals. This agrees with the experimental value. Thus we conclude that the present model with $r_{\rm cut}=1.65a_0$ can be used to predict the structural stability of fcc metals investigated though the predicted values are consistently underestimated.

In order to understand the physical origin of the structure stability, we perform calculations about the effect of cutoff distance on the structure stability for all seven metals with the potential parameters given in Table I. In the calculations, we find that the potential parameters are valid for calculating basic properties of the seven metals such as lattice constant, elastic constants, cohesive energy, and vacancy formation energy, when the cutoff distance is taken to be larger than $1.225a_0$ [third-nearest neighbor (NN)], while the potential parameters need to be refitted for a cutoff distance less than $1.225a_0$. But whether for the refitting potential parameters or for the present potential parameters, the calculated energies of the fcc-hcp stability (or fcc-bcc stability) follows the same pattern as a function of cutoff distance for all seven metals, but differs by a scaling factor. They are either positive or negative, as shown by Johnson [21]. A typical curve of the energy versus cutoff distance is plotted in Fig. 2 for Au. By further calculations we find that for all seven metals, when the cutoff distance is taken to lay in the range from $1.225a_0$ to $1.3540a_0$, or $1.5812a_0$ to $1.6833a_0$, the fcc structure is most stable where there are more atoms for the fcc than the corresponding hcp. Also, when the cutoff distance is larger than $1.225a_0$ (third NN) the fcc is always favored energetically over the bcc. We note that when the cutoff distance is taken as $1.20a_0$, which corresponds to the second NN of fcc, the third NN of bcc and hcp and the cohesive energy of hcp and bcc are larger than that of fcc. This is because that within this cutoff distance the bcc has 26 atoms, and the fcc 18 atoms. Therefore, for the EAM, where an angle force is not considered, a range of force which attains the third NN of the fcc structure is necessary for a prediction of the structure stability. In fact, we will show that to describe the fcc-hcp stability accurately a long-range force has to be considered for the EAM.

Now we plot the total energy of Au as a function of near-neighbor (NN) distance for the three structures of fcc, bcc, and hcp in Fig. 3(a). The corresponding component term, i.e., the contribution of the pair potential (or embedding

TABLE I. Metal properties used in fit and fitting parameters. Where two numbers are given, the top number is the calculated value, and the lower number is the experimental value.

| | Al | Ag | Au | Cu | Ni | Pd | Pt |
|---|---|---|---|---|---|---|---|
| $a_0$ (Å) | 4.05 | 4.09 | 4.08 | 3.615 | 3.52 | 3.89 | 3.92 |
| | 4.05[a] | 4.09[a] | 4.08[a] | 3.615[a] | 3.52[a] | 3.89[a] | 3.92 |
| $E_c$ (eV) | 3.32 | 2.83 | 3.90 | 3.52 | 4.45 | 3.88 | 5.72 |
| | 3.36[b] | 2.85[c] | 3.93[c] | 3.54[c] | 4.45[c] | 3.91[b] | 5.77[c] |
| $C_{11}$ (erg/cm$^3$) | 0.90 | 1.21 | 1.77 | 1.68 | 2.38 | 2.24 | 3.09 |
| | 1.14[d] | 1.24[d] | 1.86[d] | 1.70[d] | 2.465[d] | 2.341[c] | 3.47[d] |
| $C_{12}$ (erg/cm$^3$) | 0.702 | 0.938 | 1.50 | 1.263 | 1.78 | 1.79 | 2.59 |
| | 0.619[d] | 0.934[d] | 1.57[d] | 1.225[d] | 1.473[d] | 1.76[c] | 2.51[d] |
| $C_{44}$ (erg/cm$^3$) | 0.330 | 0.467 | 0.43 | 0.752 | 1.08 | 0.726 | 0.793 |
| | 0.316[d] | 0.461[d] | 0.42[d] | 0.758[d] | 1.247[d] | 0.712[c] | 0.765[d] |
| $E_v^f$ (eV) | 0.73 | 1.10 | 0.90 | 1.31 | 1.63 | 1.40 | 1.49 |
| | 0.75[e] | 1.10[f] | 0.90[f] | 1.30[f] | 1.60[g] | 1.40[g] | 1.50[f] |
| $X_{\rm rms}$ (%) | 6.65 | 0.02 | 0.57 | 0.13 | 6.54 | 0.27 | 1.44 |
| | | | Potential parameters | | | | |
| $\chi$ (Å$^{-1}$) | 2.50 | 3.50 | 4.00 | 3.00 | 3.10 | 4.30 | 4.30 |
| $\alpha$ (eV) | 0.0834 | 0.4420 | 0.2774 | 0.3902 | 0.3768 | 0.3610 | 0.4033 |
| $\beta$ | 7.5995 | 4.9312 | 5.7177 | 6.0641 | 6.5840 | 5.3770 | 5.6379 |
| $F_1$ (eV) | −0.1392 | 0.7684 | 0.4728 | 1.0241 | 0.8784 | 0.6185 | 0.6815 |
| $r_a$ (Å) | 3.0169 | 2.2689 | 2.4336 | 2.3051 | 2.3600 | 2.3661 | 2.3839 |

[a]Reference 35.
[b]Reference 33.
[c]Reference 36.
[d]Reference 37.
[e]Reference 34.
[f]Reference 38.
[g]Reference 39.
[h]Reference 40.

function) to the total energy (for convenience, hereafter we call them the pair potential term and embedding function term, respectively) as a function of NN distance is also exhibited in Fig. 3(b) [or Fig. 3(c)]. Figure 3(a) is equivalent to Fig. 2 because the energy of the structure stability is defined as the difference between the cohesive energies of two distinct structures, and the cutoff distance can be expressed by the NN distance (for example, the cutoff distance of $1.8a_0$ corresponds to the sixth NN of the fcc structure, the eighth NN of the bcc structure, and the ninth NN of the hcp structure). From Fig. 3 we can see that if the cutoff distance is less than the ideal hcp third-neighbor distance, the energies

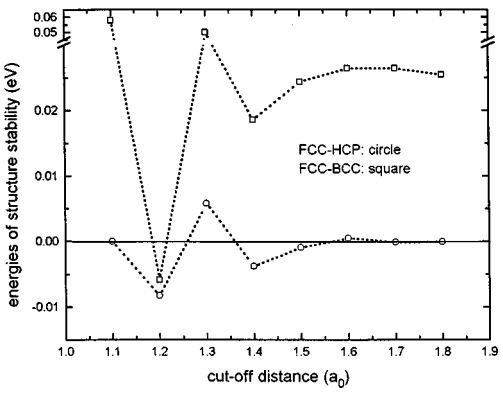


FIG. 2. Energy of the structure stability as a function of cutoff distance for metal Au. The circle-line is for the fcc-fcp stability, and the square-line is for the fcc-bcc stability.

(the total energies, or that of each of the two component terms) of the hcp and fcc lattice structures are the same. Moreover, from Figs. 3(b) and 3(c) we can observe that at long range for the pair potential and embedding function terms, the bcc has a higher energy than the fcc (or the hcp) of about 0.008 and 0.018 eV, respectively. The sum is just about the energy of the fcc-bcc stability [see Table II or Figs. 2 and 3(a)]. From these figures, we can also see that the difference between pair potential terms of the fcc and hcp structures [see Fig. 3(b)] is almost the same as that between their total energies [see Fig. 3(a)] for all near-neighbor distances considered, while the difference between embedding function terms of the fcc and hcp structures is approximately equal to zero. These can be understood, i.e., (i) if the embedding energy is a slow changing function of the host density; (ii) if the increase of the host electron density due to including the atoms away well from the nearest neighbor can almost be neglected for the three structures (fcc, bcc, and hcp); or (iii) if for the first two near neighbors the fcc structure has the same distance and number of atoms as the hcp. Hence the large difference between the host electron densities of the bcc and fcc structures results in an obvious deviation in their embedding energies, while almost the same host electron densities for the fcc and hcp lead to their embedding energies being almost the same. Due to these, compared with the pair potential, the contribution of the embedding energy to the energy of the fcc-hcp stability can be neglected, while it cannot for fcc-bcc stability. This indicates that the variation of the energies (see Fig. 2) of the fcc-bcc stability is dominated by both the embedding energy and pair potential, and

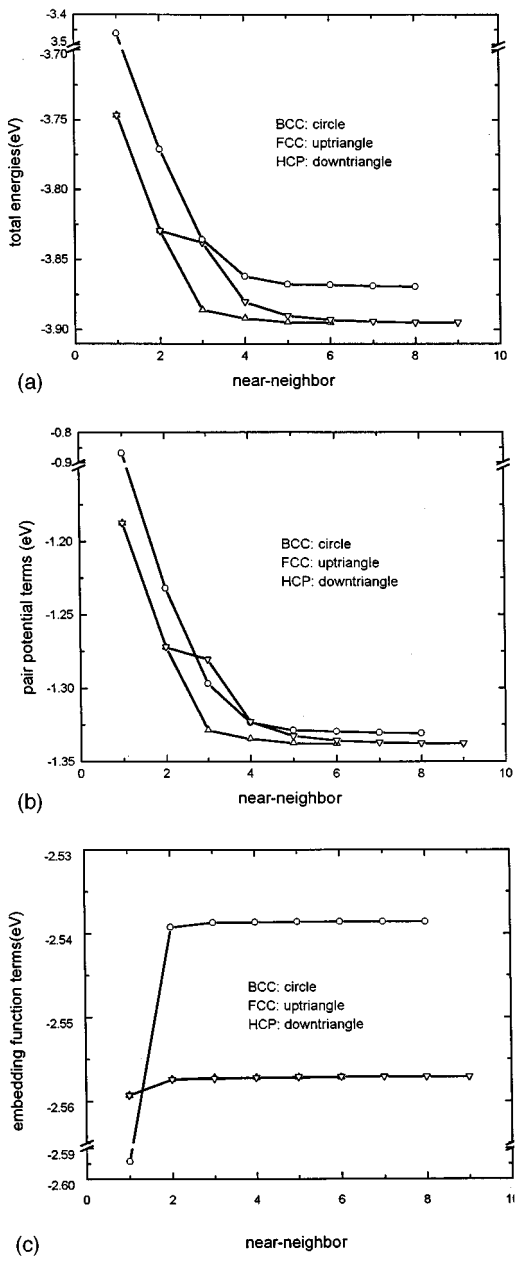


FIG. 3. (a) Total energy as a function of near-neighbor distance for metal Au. The circle is for bcc, the down triangle for hcp, and the up triangle for fcc. (b) Pair potential term as a function of near-neighbor distance for metal Au. The circle is for bcc, the down triangle for hcp, and the up triangle for fcc. (c) Embedding function term as a function of near-neighbor distance for metal Au. The circle is for bcc, the down triangle for hcp, and the up triangle for fcc.

by only the pair potential for the fcc-hcp stability. The former is obvious, and can be seen from Fig. 3, while the latter may give rise to some question due to the small value of energy of the fcc-hcp stability (see Table II). The latter can be illustrated by more detailed results. When the cutoff distance is taken as $r_{\rm cut}=1.20a_0$, which corresponds to the second NN of the fcc structure and the third NN of the hcp structure, the energy of the fcc-hcp stability of Au is found to be $-0.008$ eV. The contribution of the pair potential to this energy is $-0.008$ eV, while the contribution of the embedding energy to the energy is found to be equal to $5.3\times10^{-5}$ eV. Hence, compared with the pair potential, the contribution of the embedding energy to the energy of the fcc-hcp stability can be neglected. Our calculations show that this conclusion does not depend on the choice of cutoff distance and material. This conclusion should be valid for all EAM models where the atomic electron density has a rapidly decreasing form and the angle force is not considered.

We have shown that the energy of the fcc-hcp stability is underestimated using our present EAM potential. Therefore, in order to increase the energy of the fcc-hcp stability we should include the contribution of the embedding function to the stability. This may be completed by considering the dependence of the atomic electron density on angle. With this electron density the difference between the host electron densities of the fcc and hcp should occur for the first two near neighbors, and this will lead to a difference between the embedding energies. Of course, a long-range pair potential can also be used to improve the structure stability. This point can be illustrated by making a comparison between fcc and hcp structures. At the first two near neighbors the fcc and hcp have the same atoms and near-neighbor distance, while between the second- and third-nearest neighbors of fcc ($r_{\rm cut}=1.154\,71a_0$) the corresponding hcp has two atoms. The third-nearest neighbor of the fcc ($r_{\rm cut}=1.22475a_0$) has 24 atoms, and corresponds to the fourth-nearest neighbor of the hcp. The fourth-nearest neighbor of the hcp has 18 atoms. Thus at a cutoff distance of $r_{\rm cut}=1.154\,71a_0$ the hcp has two more atoms than the fcc, while at $r_{\rm cut}=1.224\,75a_0$ the fcc has six more atoms than the hcp. Hence the energy of the fcc-hcp stability depends on the competition between the six atoms of the fcc and the two atoms of the hcp. In this situation, in order to make the fcc is more stable than the hcp, the pair potential has to change slowly between the distances of $1.154\,71a_0$ and $1.2247a_0$. This slow change requires a small $\beta$ appearing on Eq. (5), i.e., the pair potential should be a long-range one. The following example may let one more clearly understand this point.

We use the potential parameters listed in Table I to calculate the energy of the fcc-hcp stability with a cutoff distance of $r_{\rm cut}=1.65a_0$. The energy is found to be underestimated. However, if we refit the potential parameters by forcing the total internal energy of a fcc metal (say, Au) is lower by 0.005 eV (the experimental value) than the total internal energy of the hcp, we obtain the refitting potential parameters $\alpha=0.5317$ eV, $\beta=1.9324$, $\chi=4.60$ Å$^{-1}$, $F_1=0.3681$ eV, and $r_a=1.2714$ Å. This fitting error is $X_{\rm rms}=3.6\%$. Using these refitting parameters to calculate the energy of the fcc-hcp stability, the fcc is energetically favored over the hcp by 0.0042 eV (over the bcc by 0.033 eV). Thus in this situation our present EAM model predicts that the fcc-hcp stability (or the fcc-hcp stability) is in good agreement with the experimental value of 0.005 eV (or 0.04 eV). However, we note that the refitting $\beta=1.9324$ is far smaller than the $\beta=5.7177$ given in Table I. This results in that the refitting pair potential with $\beta=1.9324$ has a longer range than the previous fitting one with $\beta=5.7177$. For the other six metals we also have a similar conclusion. Therefore, for an EAM where an angle force is not included, in order to predict the fcc-hcp stability accurately a long-range pair potential needs to be considered. One may conclude that

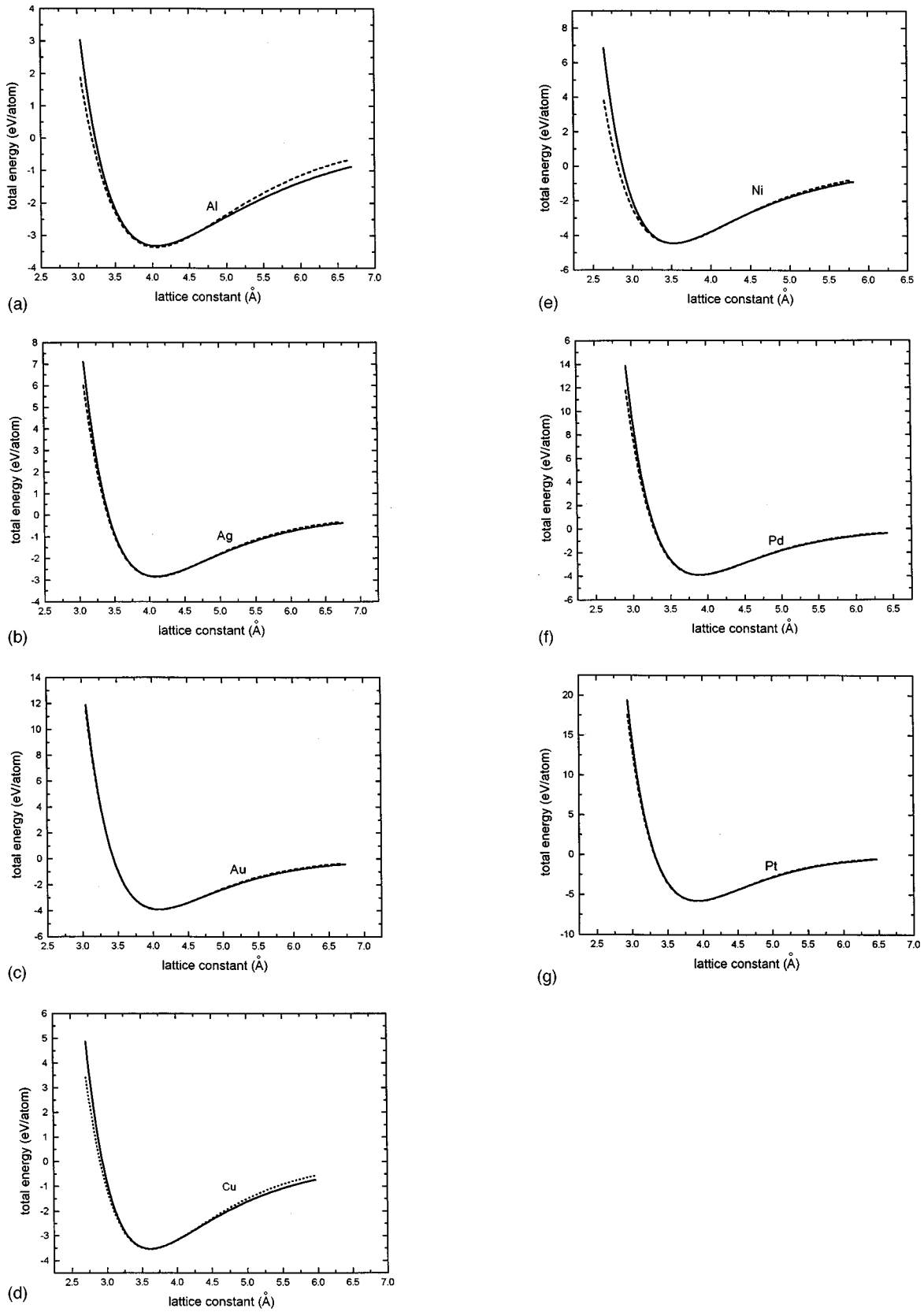


FIG. 4. Equations of state for metals Al, Ag, Au, Cu, Ni, Pd, and Pt. The solid curves are from the present model, and the dashed curves are from Rose *et al.* (Ref. 6).

by a similar consideration of long-range atomic electron density, the fcc-hcp stability should also be correctly predicted. However, we will see in the following that a smaller value of $\chi$ appearing in Eq. (3) can yield a serious deviation of the calculated total energy of the present EAM model from the equation of state of Rose *et al.* A deeper insight into the origin of the physics of structure stability should cast more level calculations. Skriver[22] has shown that one-electron

theory can be used to explain the stability of metals over a wide range.

We have discussed the stability of crystal structure for all seven metals. We now calculate the equation of state of the total energy as a function of the lattice constant. As is well known, the study of alloys or defects such as dislocations and interstitials requires a knowledge of the interatomic potential at distances very different from the equilibrium one. Therefore the total-energy dependence of the lattice constant has to be compared with the equation of state of Rose *et al.* Rose *et al.*[6] have shown that the sublimation energy of most metals as a function of lattice constant can be correctly described by the equation. The predictions of our model are compared in Fig. 4 with the calculated results from the equation of state of Rose *et al.* for Al, Ag, Au, Cu, Ni, Pd, and Pt. The predicted results of our model are in good agreement with those from the equation of state of Rose *et al.* The agreement is best for Pt, Pd, and Au, and Ag, medium for Cu and Ni, and fair for Al. We find the agreement is closely related to the contribution of the atoms of the second-nearest neighbor to the host density. We obtain that this contribution is equal to 0.309, 0.091, 0.053, 0.251, 0.246, 0.045, and 0.043 for Al, Ag, Au, Cu, Ni, Pd, and Pt, respectively. According to these results we conclude that the lower the contribution of the atoms of the second-nearest neighbor to the host density, the better the agreement [the larger the value of $\chi$ appearing in Eq. (3), the less the contribution of the atoms of the second near neighbor to the host electron density). This can be understood by considering the relationship among the universal embedding energy, the host density, and the model function of Rose *et al.* If the atomic electron density is assumed to be a decreasing exponential function the lower the contribution of the atoms of the second-nearest neighbor to the host electron density is, the more similar decreasing exponential form the summation of atomic electron density [i.e., the host electron density [see Eq. (3)]] has. Benearjea and Smith[17] have shown that a host density with a decreasing exponential form incorporating the universal embedding energy may lead to the model function of Rose *et al.* Therefore, the agreement between the calculated total energy and the equation of state of Rose *et al.* should be better if the contribution of atoms of the second-nearest neighbor to the host electron density is less. A detailed example can be used to interpret this point. We refit the properties of Ni by requiring $X_{\rm rms}$ to be smaller than 3.0%, and we obtain the potential parameters of $\alpha=0.1438$ eV, $\beta=8.0235$, $\chi=2.50$ Å$^{-1}$, $F_1=-0.6945$ eV, and $r_a=2.6759$ Å. We find that though the fitting accuracy is improved for the calculation of the properties of metal Ni at equilibrium, the total energy as a function of lattice parameter cause a more serious deviation from the equation of state of Rose *et al.* than the one displayed in Fig. 4(e). This is due to the fact that $\chi=2.50$ Å$^{-1}$ is smaller than 3.10 Å$^{-1}$ (see Table I), and using $\chi=2.5$ Å$^{-1}$ to calculate the contribution of atoms of the second-nearest neighbor to the host density is found to be equal to 0.456, which is larger than 0.246 obtained using $\chi=3.10$ Å$^{-1}$. It should be emphasized that in our fitting we do not sacrifice accuracy for calculating the properties at equilibrium so as to satisfy the equation of state of Rose *et al.* for the other six metals. Foiles, Baskes, and Daw have emphasized[5] that the set of functions in the EAM should be good when they can reproduce the Rose *et al.* model function well.

### B. Vacancy formation energy at (111) surface and divacancy binding energy

A direct application to the divacancy binding energy can further illustrate the reliability of the present potential model. The divacancy binding energy is the difference between the energies of two well-separated vacancies and two first-neighbor vacancies. For the unreleased divacancy we can write the binding energy $E_{2v}^b$ as

$$E_{2v}^b=2E_v^f-\left(\sum_{i\geqslant 3}^{N}[F_i(\rho_e-f(r_{1i})-f(r_{1i}))-F_i(\rho_e)]+\phi(r_e)-\sum_{i(\neq 1)}\phi(r_{1i})\right), \tag{6}$$

where, without loss of generality, we assume that the two first-neighbor vacancies are produced in the lattice positions of two the nearest atoms, i.e., atoms 1 and 2; $E_v^f$ is the unreleased vacancy formation energy; and $r_e$ is the equilibrium nearest distance. The predictions of the binding energy of divacancies is reported in Table II using Eq. (6). A positive value indicates an attraction between the vacancies. The calculations are in very good agreement with the experimental values, with the exceptions of Pt and Cu, for which the calculated binding energy is larger than the experimental estimates.

Our present model is also used to calculate the vacancy formation energy at the (111) surfaces for all seven metals. The surface-vacancy formation energy is the lowest energy required to remove an atom from the surface, and usually the atom is brought to a reservoir which determines the atomic chemical potential. For crystals built from only a single species the chemical potential is the cohesive energy.[23] The physics behind this is that the removed atom is brought to step and kink sites, and the step or the kink will not be changed. In other words, adsorbing metal atom at a kink site of a realistic metal surface releases an energy equal to the bulk cohesive energy. The unrelaxed surface-vacancy-formation energy then is

$$E_{\rm vac(111)}^f=\tfrac{1}{2}(E_{\rm vac(111)}-2E_c-E_{(111)}), \tag{7}$$

where $E_{(111)}$ is the total energy of a thin slab with (111) surfaces, $E_{\rm vac(111)}$ is the total energy of the slab where a vacancy is created at each surface, and $E_{\rm vac(111)}^f$ denotes the vacancy formation energy at the (111) surface. The calculated values for the surface-vacancy-formation energies are given in Table II along with the available results from the first-principles calculations.[23,24] The agreement between the present calculations and the first-principles calculations is satisfactory.

### C. Surface relaxation and surface energy

We have calculated the divacancy binding energy, the cohesive energies of the fcc, hcp, and bcc and the equation of state, and the surface-vacancy-formation energies. All the above results are in reasonable accordance with experimental

TABLE II. The energy of structure stability, vacancy formation energy at the (111) surface, and the divacancy binding energy.

| | Al | Ag | Au | Cu | Ni | Pd | Pt |
|---|---|---|---|---|---|---|---|
| $E_{fcc}$-$E_{bcc}$ (eV) | 0.0168 | 0.0254 | 0.0265 | 0.0220 | 0.033 | 0.0370 | 0.0430 |
| | 0.10[a] | 0.03[a] | 0.04[a] | 0.04[a] | 0.07[a] | 0.10[a] | 0.15[a] |
| $E_{fcc}$-$E_{hcp}$ (eV) | 0.0003 | 0.0012 | 0.0005 | 0.0012 | 0.0010 | 0.0016 | 0.0011 |
| | 0.05[a] | 0.003[a] | 0.005[a] | 0.006[a] | 0.015[a] | 0.02[a] | 0.02[a] |
| $E^b_{2v}$ (eV) | 0.16 | 0.40 | 0.30 | 0.48 | 0.55 | 0.45 | 0.48 |
| | | 0.38[b] | 0.2–0.6[c] | 0.12[d] | 0.33[e] | | 0.1–0.2[c] |
| $E^f_{vac(111)}$ (eV) | 0.42 | 0.53 | 0.51 | 0.64 | 0.81 | 0.69 | 0.81 |
| | 0.36,[f]0.66[g] | 0.67[f] | | 0.92[f] | | | |

[a]Reference 4.
[b]Reference 41.
[c]Reference 39.
[d]Reference 42.
[e]Reference 43.
[f]Reference 24.
[g]Reference 23.

data or the results from first-principles calculations. Further, we will investigate the multilayer relaxation of surfaces for the metals Al, Ag, Au, Cu, Ni, Pd, and Pt using our present EAM model (see Tables III and IV).

In this study the surface energy and the geometry of the low-index faces (100), (110), and (111) are calculated. The surface energy is the energy difference between the energy of a periodic slab of atoms and the energy of the same number of atoms in the bulk metal. In all cases, the relaxation of each atom layer parallel to the surface is allowed to occur. This is performed by minimizing the total energy of the slabs. The slabs are sufficiently thick to guarantee that the surface energies and geometries are independent of the thickness. In the calculation we have not made any effort to search for an energetically favored reconstruction. The EAM is a good tool for the investigation of reconstruction, though.

The surface energies obtained for the low-index faces of these seven metals are presented in Table III, and the results from first-principles calculations,[25] or from experiments[26] are also included in this table. For all cases, the close-packed (111) face has the lowest energy, followed by the (100) and (110) faces. The trend is in good agreement with first-principles calculations, but the calculated values, compared with experimental data or the first-principles calculation, are consistently too small. This is a common conclusion whether these calculations are from Refs. 5, 12, or 27. Therefore, in the theoretical framework of the EAM for a more accurate calculation of surface energy the EAM should include a correction involving electron density, as Daw pointed out[19] and Baskes showed.[4] We will extend our present EAM model to consider this point in the sequel to this paper.

TABLE III. Surface energies (in the unit of erg/cm$^2$) for seven pure metals. The first row is the results predicted by the present EAM model. The second row is those from the first-principles calculations of Skriver and Rosengaard (Ref. 25). The experimental values correspond to average surface energies, which are from Ref. 26.

| | Al | Ag | Au | Cu | Ni | Pd | Pt |
|---|---|---|---|---|---|---|---|
| (100) | 579 | 821 | 683 | 1261 | 1654 | 1157 | 1228 |
| | | 1200 | 1710 | 2090 | | 1900 | 2480 |
| (110) | 627 | 883 | 728 | 1361 | 1786 | 1240 | 1309 |
| | | 1290 | 1790 | 2310 | | | |
| (111) | 524 | 765 | 618 | 1180 | 1540 | 1074 | 1120 |
| | 1270 | 1120 | 1610 | 1960 | 2630 | 1880 | 2350 |
| Expt. | 1160 | 1250 | 1500 | 1830 | 2450 | 2050 | 2480 |

The change in interlayer spacing $\Delta z$'s for the relaxed (110), (100), and (111) surfaces of the seven metals are calculated using the present potential mode, and a comparison between the theoretical results and experimental data is presented in Table IV. As shown in Table IV, for relaxations of (100), (110), and (111) faces, our model gives comparable magnitudes in interlayer spacings to the experimental or more level calculations. Note that all top-layer spacings show a small contraction. Further, the rougher (110) surfaces show a larger relaxation than the smoother (100) and (111) faces do. In addition, for (110) surfaces the relaxation shows an oscillating behavior of contraction-dilation-contraction. These general features agree with the trends found in the experiment, or with results from more level calculations.

### D. Alloy and impurities

The present model has been used to investigate pure metal systems, and the results are satisfactory. However, one of the attractive features of the EAM formalism is that it has a form that can be applied directly to metallic alloys. Here we will show that our model can be used to investigate the alloy systems.

In an EAM model, for a binary alloy system with type-$a$ atoms and type-$b$ atoms, there exist two kinds of electron density functions $f_a(r)$ and $f_b(r)$, two kinds of embedding energy functions $F_a(\rho)$ and $F_b(\rho)$, and three kinds of pair potential functions $\phi_{aa}(r)$, $\phi_{bb}(r)$, and $\phi_{ab}(r)$. Usually the six functions $f_a(r)$, $f_b(r)$, $F_a(\rho)$, $F_b(\rho)$, $\phi_{aa}(r)$, and $\phi_{bb}(r)$ are assumed to be transferable from monatomic systems to alloy systems. The remaining function $\phi_{ab}(r)$ is assumed to be the geometric mean of monatomic pair potentials by the model of Foiles, Baskes, and Daw,[5] or alternatively to be a density-weighted combination of monatomic pair potentials by the model of Johnson.[8] The former

TABLE IV. Surface relaxation of the top-layer spacing $\Delta z$'s for the low-index faces (in unit of Å%).

| | | Al | Ag | Au | Cu | Ni | Pd | Pt |
|---|---|---|---|---|---|---|---|---|
| (100) | $\Delta z_{12}$ | $-4.98$ | $-1.55$ | $-6.69$ | $-0.43$ | $-0.76$ | $-2.84$ | $-5.55$ |
| | | $-3$[a] | 0[b] | 0[b] | $-1.1$[c] | $-3.2$[d] | | $<\|0.2\|$[e] |
| | $\Delta z_{23}$ | $-0.015$ | 0.15 | 1.10 | 0.03 | $-0.05$ | 0.33 | 0.866 |
| | | 0[a] | | 1.7[b] | $+1.7$[c] | | | |
| | $\Delta z_{34}$ | 0.014 | 0.004 | 0.168 | $-0.00$ | 0.00 | $-0.024$ | 0.128 |
| (110) | $\Delta z_{12}$ | $-10.2$ | $-5.39$ | $-12.5$ | $-3.60$ | $-3.77$ | $-6.89$ | $-9.18$ |
| | | $-7.0$[a] | $-5.7$[f] | | $-8.5$[g] | $-8.7$[h] | $-6.0$[i] | |
| | $\Delta z_{23}$ | 1.20 | 0.88 | 2.43 | 0.45 | 0.41 | 1.02 | 2.07 |
| | | | $+2.0$[f] | | $+2.3$[g] | $+3.0$[h] | $+1.0$[i] | |
| | $\Delta z_{34}$ | $-0.71$ | $-0.31$ | $-0.53$ | $-0.34$ | $-0.33$ | $-0.0414$ | $-0.506$ |
| | | | $-3.5$[f] | | | $-0.5$[h] | | |
| (111) | $\Delta z_{12}$ | $-4.18$ | $-1.71$ | $-5.06$ | $-1.17$ | $-1.32$ | $-2.402$ | $-4.23$[l] |
| | | $-1$[a] | $<\|2\|$[j] | 0[b] | $-0.7$[k] | 0[b] | | $<\|0.4\|$ |
| | $\Delta z_{23}$ | 0.18 | 0.1 | 0.74 | 0.001 | 0.00 | 0.203 | 0.567 |
| | | 0[a] | | | | | | |
| | $\Delta z_{34}$ | $-0.007$ | $-0.006$ | $-0.099$ | 0.001 | 0.00 | $-0.011$ | $-0.074$ |

[a]Reference 18.
[b]Reference 46.
[c]Reference 47.
[d]Reference 50.
[e]Reference 53.
[f]Reference 44.
[g]Reference 48.
[h]Reference 51.
[i]Reference 52.
[j]Reference 45.
[k]Reference 49.
[l]Reference 54.

alloy potential model is imaginary if one of the monatomic two-body potentials is negative and the other positive. The latter alloy potential model has been proven to be invariant for transformations in the monatomic model from which they are derived, and this invariance holds for any number of different elements in an alloy.[8] The alloy model of Johnson has been applied to fcc- and bcc-based binary alloys.[9,28] We will use the density-weighted model to investigate the dilute-limit heats of solution, and the heats of formation of a fcc-based binary alloy in our present calculations.

TABLE V. Dilute-limit heat of solution of 42 alloys. The first rows are from the present calculation, and the second rows are from the experiment (Ref. 29). The data with asterisks are from Mediema alloy theory calculations (Ref. 30). All energies are in eV.

| | Host | | | | | | |
|---|---|---|---|---|---|---|---|
| | Al | Ag | Au | Cu | Ni | Pd | Pt |
| Al | | $-0.50$ | $-0.96$ | $-1.77$ | $-2.08$ | $-2.92$ | $-1.14$ |
| Ag | $-0.61$ | | $-0.11$ | 0.04 | 0.50 | $-0.32$ | 0.13 |
| | $-0.23$* | | $-0.16$ | 0.39 | | $-0.11$ | |
| Au | $-1.11$ | $-0.10$ | | $-1.07$ | 0.17 | $-0.33$ | 0.26 |
| | $-0.98$* | $-0.19$ | | $-0.19$ | | $-0.20$ | |
| Cu | $-1.29$ | 0.07 | $-0.37$ | | 0.05 | $-2.28$ | $-1.51$ |
| | $-0.33$* | 0.25 | $-0.13$ | | 0.11 | $-0.39$ | $-0.30$ |
| Ni | $-1.30$ | 0.49 | 0.11 | 0.04 | | $-1.65$ | $-1.24$ |
| | $-0.84$* | | 0.22 | 0.03 | | $-0.09$ | $-0.33$ |
| Pd | $-3.25$ | $-0.29$ | $-0.29$ | $-2.85$ | $-2.54$ | | $-0.21$ |
| | $-1.94$* | $-0.29$ | $-0.36$ | $-0.44$ | 0.06 | | |
| Pt | $-1.54$ | 0.19 | 0.25 | $-2.32$ | $-2.58$ | $-0.19$ | |
| | | | | $-0.53$ | $-0.28$ | $-0.04$ | |

In the density-weighed model it is necessary to know the electron-density scaling factor $f_e$. Johnson pointed out that the factor can be determined by the relationships $f_e = E_c/\Omega$. The physical reality is that the electron density is proportional to the cohesive energy and inversely proportional to the atomic volume. In our present calculations a slight modification should be made for the scaling factor, i.e., $f_e$ is assumed to be equal to $(E_c/\Omega)^{\gamma}$. $\gamma$ is an adjustable parameter to be determined by the dilute-limit heats of solution. We find that the dilute-limit heats of solution can be well described when $\gamma$ is taken as 0.8 for Cu and Ni, 1.0 for Pd and Pt, 1.1 for Ag and Au, and 1.65 for Al, but there is a special case in which $\gamma$ should be taken as 0.6 for Al in the alloys involving Ni or Cu, and 0.3 for Ni in the alloys involving Au.

The dilute-limit heat of solution for a guest atom of type $b$ in a host lattice with $a$-type atoms can be calculated as the summation of the following four terms: (1) the energy required to form a vacancy in the bulk of $a$-type atoms; (2) the energy needed to move a $b$-type atom from the bulk of $b$-type atoms to infinite to form an isolate $b$-type atom; (3) the energy released to put the isolated $b$-type atom into the position of the vacancy produced in the first step; and (4) a volume relaxation energy. Following Johnson[8] this volume relaxation energy can be determined by the relationship of $E_{\rm vol} = -[1.167(\Omega_a/\Omega_b - 1)]^2$, where $\Omega_a$ and $\Omega_b$ correspond to the $a$- and $b$-type atom volumes, respectively, and $E_{\rm vol}$ is the volume relaxation energy. The heats of solution for all combinations of the seven fcc elements Al, Ag, Au, Cu, Ni, Pd, and Pt are given in Table V, together with the available experimental data.[29] In addition, the data for alloys involving metal Al from Miedema alloy theory[30] are also

TABLE VI. Heats of formation and lattice constants. The first rows are the results from the present calculations, the second rows are data from first-principles calculations (Refs. 31, 32, and 10) excluding the data of $AB$-type compounds containing metal Al, where the values are from Miedema theory calculations (Ref. 30). The values with asterisks are from the prediction of Vegard law.

| System | $a_0$ (Å) | $\Delta E$ (eV) | System | $a_0$ (Å) | $\Delta E$ (eV) | System | $a_0$ (Å) | $\Delta E$ (eV) | System | $a_0$ (Å) | $\Delta E$ (eV) |
|---|---|---|---|---|---|---|---|---|---|---|---|
| $AlAg_3$ | 4.089 | −0.08 | $AlAu_3$ | 4.081 | −0.17 | $AlCu_3$ | 3.705 | −0.31 | $AlNi_3$ | 3.622 | −0.35 |
| | 4.080* | | | 4.073* | | | 3.724* | | | 3.573 | −0.41 |
| AlAg | 4.082 | −0.12 | AlAu | 4.079 | −0.23 | AlCu | 3.803 | −0.39 | AlNi | 3.740 | −0.43 |
| | 4.070* | −0.10 | | 4.065* | −0.38 | | 3.833* | −0.18 | | 3.785* | −0.49 |
| $Al_3Ag$ | 4.070 | −0.09 | $Al_3Au$ | 4.076 | −0.17 | $Al_3Cu$ | 3.917 | −0.28 | $Al_3Ni$ | 3.879 | −0.30 |
| | 4.060* | | | 4.058* | | | 3.941* | | | 3.918* | |
| $AlPd_3$ | 3.970 | −0.44 | $AlPt_3$ | 3.991 | −0.14 | $AgAu_3$ | 4.0 | −0.03 | $AgCu_3$ | 3.744 | 0.06 |
| | 3.930* | | | 3.953* | | | 4.060 | −0.18 | | 3.680 | 0.34 |
| AlPd | 4.012 | −0.64 | AlPt | 4.034 | −0.21 | AgAu | 4.076 | −0.03 | AgCu | 3.873 | 0.08 |
| | 3.970* | −0.87 | | 3.985* | | | 4.046 | −0.24 | | 3.800 | 0.47 |
| $Al_3Pd$ | 4.038 | −0.48 | $Al_3Pt$ | 4.065 | −0.15 | $Ag_3Au$ | 4.0 | −0.02 | $Ag_3Cu$ | 3.992 | 0.05 |
| | 4.010* | | | 4.018* | | | 4.038 | −0.18 | | 3.920 | 0.36 |
| $AgNi_3$ | 3.668 | 0.16 | $AgPd_3$ | 3.935 | −0.03 | $AgPt_3$ | 3.956 | 0.05 | $AuCu_3$ | 3.697 | −0.17 |
| | 3.663* | 0.26 | | 3.940* | −0.01 | | 3.963* | 0.10 | | 3.70 | −0.26 |
| AgNi | 3.822 | 0.21 | AgPd | 3.980 | −0.05 | AgPt | 3.994 | 0.07 | AuCu | 3.823 | −0.15 |
| | 3.805* | 0.34 | | 3.990* | −0.02 | | 4.005* | 0.18 | | 3.84 | −0.28 |
| $Ag_3Ni$ | 3.967 | 0.15 | $Ag_3Pd$ | 4.032 | −0.03 | $AgPt_3$ | 4.039 | 0.06 | $Au_3Cu$ | 3.959 | −0.07 |
| | 3.948* | 0.22 | | 4.040* | −0.04 | | 4.048* | 0.10 | | 3.96 | −0.14 |
| $AuNi_3$ | 3.680 | 0.11 | $AuPd_3$ | 3.937 | −0.06 | $AuPt_3$ | 3.961 | 0.07 | $CuNi_3$ | 3.543 | 0.01 |
| | 3.660* | 0.05 | | 3.938* | −0.06 | | 3.960* | 0.08 | | 3.544* | 0.02 |
| AuNi | 3.845 | 0.15 | AuPd | 3.983 | −0.08 | AuPt | 4.000 | 0.08 | CuNi | 3.566 | 0.02 |
| | 3.800* | 0.06 | | 3.985* | −0.11 | | 4.000* | 0.11 | | 3.568* | 0.04 |
| $Au_3Ni$ | 3.982 | 0.10 | $Au_3Pd$ | 4.031 | −0.06 | $Au_3Pt$ | 4.040 | 0.06 | $Cu_3Ni$ | 3.591 | 0.01 |
| | 3.940* | 0.05 | | 4.033* | −0.10 | | 4.040* | 0.06 | | 3.591* | 0.01 |
| $CuPd_3$ | 3.797 | −0.39 | $CuPt_3$ | 3.820 | −0.31 | $NiPd_3$ | 3.772 | −0.29 | $NiPt_3$ | 3.790 | −0.29 |
| | 3.821* | −0.06 | | 3.844* | −0.14 | | 3.798* | | | 3.820* | |
| CuPd | 3.705 | −0.56 | CuPt | 3.719 | −0.49 | NiPd | 3.654 | −0.47 | NiPt | 3.668 | −0.52 |
| | 3.752* | −0.08 | | 3.768* | −0.12 | | 3.705* | | | 3.720* | |
| $Cu_3Pd$ | 3.637 | −0.46 | $Cu_3Pt$ | 3.641 | −0.42 | $Ni_3Pd$ | 3.563 | −0.41 | $Ni_3Pt$ | 3.567 | −0.48 |
| | 3.684* | −0.09 | | 3.691* | −0.12 | | 3.613* | | | 3.620* | |
| $PtPd_3$ | 3.896 | −0.04 | PtPd | 3.903 | −0.05 | $PdPt_3$ | 3.911 | −0.03 | | | |
| | 3.898* | | | 3.905* | | | 3.913* | | | | |

included in this table. The general agreement (excluding the values of impurity Pd in host Ni) can be seen in the table. The dilute-limit heats of solution of binary systems containing Pd predicted by Johnson have remarkable disagreements with experimental data, i.e., the wrong trends are predicted for the properties of the dilute-limit heats of solution of alloys involving Pd (see Table II in Ref. 8). With the present method, this wrong is cancelled except for the case of Pd in Ni.

The heats of formation of an alloy is the difference of the total cohesive energies between the alloy and their pure constituents. We calculate the heats of formation for all intermetallic compounds of the seven fcc metals to form an $A_3B$-type alloy with $L1_2$ structure, a $B_3A$-type alloy with $L1_2$ structure, and an $AB$-type alloy with $L1_0$ structure. We do not consider the tetragonal distortion of an $L1_0$ superstructure. The calculated heats of formation and lattice constants for the 63 binary alloys together with available data from the first-principles calculations[31,32] are summarized in Table VI. Compared with the first-principles calculations, the results are good for Cu-Ni, Ag-Pd, Au-Pd, Au-Pt, Ag-Pt, Ag-Ni, and $Ni_3Al$ alloy systems, fair for Au-Ni and Cu-Au alloy systems, and weak for Cu-Pt, Cu-Pd, Cu-Ag, and Ag-Au alloy systems in magnitude. All calculated values are in qualitative agreement with first-principles calculations. The other results involving metal Al can be compared with the data from Miedema alloy theory.[30] The agreement is also found to be good for the alloys AlNi, AlAg, and AlPd, and fair for the alloys AlCu and AlAu. Unlike the model of Johnson, where the heats of formation are predicted to be opposite to the results of first-principles calculations for the alloy containing metal Pd (see Fig. 1 in Ref. 9), our present model resolves these problems of Johnson's. In general, for our present model the weak results can be improved by a

special choice of $\gamma$ for a special alloy. For example, we take $\gamma=0.6$ for Au and $\gamma=1.1$ for Ag. We obtain the heats of formation of $Au_3Ag$, AuAg, and $Ag_3Au$ to be equal to $-0.16$, $-0.23$, and $-0.17$ eV, respectively. These results are in excellent agreement with those from first-principles calculations ($-0.18$ eV for $Ag_3Ag$ and $Ag_3Au$, and $-0.24$ eV and for AgAu), though in this situation the calculated dilute-limit heats of solution are underestimated by the $\gamma$ parameters for the Ag-Au system. Finally, we compare the calculated lattice constants with those from the first-principles calculation or the prediction of Vegard law. The agreement can be also found to be good in Table VI. In addition, we use the refitting potential parameters of Ni ($\alpha=0.1438$ eV, $\beta=8.0235$, $\chi=2.50$ Å$^{-1}$, $F_1=-0.6945$ eV, and $r_a=2.6759$ Å) to calculate the properties of alloys involving metal Ni. Our results show that the dilute-limit heats of solution and the heats of formation of the alloys involving metal Ni are predicted to be bad. This may result from bad properties of metal Ni at the nonequilibrium (i.e., the deviation of calculated total energy from the equation of state of Rose *et al.*).

## IV. CONCLUSION

We give a simple and analytical EAM model for fcc metals. The model includes a long-range force. In this model, the electron-density function is taken as a decreasing exponential function, the two-body potential is defined as a function like a form given by Rose *et al.*, and the embedding energy is assumed to be a universal form recently suggested by Banerjea and Smith. The potential parameters of this model are determined by fitting pure metal bulk properties such as lattice constant, elastic constants, cohesive energy, and vacancy formation energy. The model does not require more rigorous development than a pair potential. The model is applied to seven fcc metals and all their binary alloys. For pure metal systems, the properties of the seven metals Al, Ag, Au, Cu, Ni, Pd, and Pt, including the equation of state of total energy V s lattice constant, divacancy binding energy, surface energy, surface relaxation, and vacancy formation energies at the (111) surface, are calculated. In all cases, the results are in reasonable agreement with the experimental data or the data from first-principles calculation. In addition, the two energies of fcc-hcp and fcc-bcc stabilities are also calculated. It is found that the energy of the fcc-hcp stability is dominated by only the pair potential, and is underestimated while the energy of the fcc-bcc stability is dominated by both the pair potential and embedding energy. Likewise, by calculating the total energy of the seven metals, we find that the present EAM model predicts the total energy as a function of the lattice parameter to be in good agreement with the equation of state of Rose *et al.* This agreement is closely related to the electron density, i.e., the lower the contribution from atoms of the second-nearest neighbor to the host density, the better the agreement becomes. These results are discussed in detail. Thus we obtain that (i) for an EAM, where angle force is not considered, a long-range force is necessary for the prediction of the structure stability; and (ii) the dependence of the electron density on angle should be considered for increasing the energy of the fcc-hcp stability. Our present model may be easy to use to make this extension. For alloy systems, the heats of formation of the intermetallic compounds of $A_3B$, $AB$, and $AB_3$, which consist of the seven pure metals, are predicted to be in agreement with first-principles calculations or the data from Miedema alloy theory, and the dilute-limit heats of solution are also generally well represented by the present potential except for the case of impurity Pd in host Ni. Moreover, the lattice constants of the intermetallic alloys are predicted to be in agreement with these from Vegard law or from the first-principles calculations. The present potential model solves the disagreement between the experimental and calculated data by Johnson's potential model for phase stability and dilute-limit heats of solution of the alloy systems with palladium.[8,9]

## ACKNOWLEDGMENT

The research was supported by the Natural Science Foundation of China.

[1] M. S. Daw and I. Baskes, Phys. Rev. B **29**, 6443 (1984); Phys. Rev. Lett. **50**, 1285 (1983).
[2] M. W. Finnis and J. E. Sinclair, Philos. Mag. A **50**, 45 (1984).
[3] P. Hohenberg and W. Kohn, Phys. Rev. B **136**, 864 (1964).
[4] M. I. Baskes, Phys. Rev. B **46**, 2727 (1992).
[5] S. M. Foiles, M. I. Baskes, and M. S. Daw, Phys. Rev. B **33**, 7983 (1986).
[6] J. H. Rose, J. R. Smith, F. Guinea, and J. Ferrante, Phys. Rev. B **29**, 2963 (1984).
[7] R. A. Johnson, Phys. Rev. B **37**, 3924 (1988).
[8] R. A. Johnson, Phys. Rev. B **39**, 12 554 (1989).
[9] R. A. Johnson, Phys. Rev. B **41**, 9717 (1990).
[10] A. F. Voter and S. P. Chen, in *Characterization of Defects in Materials*, edited by R. W. Siegal, J. R. Weetman, and R. Sinclair, MRS Symposia Proceedings No. 82 (Materials Research Society, Pittsburgh, 1987), p. 175.
[11] F. Ercolessi, E. Tosatti, and M. Parrinello, Surf. Sci. **177**, 314 (1986).
[12] V. Rosato, M. Guilope, and B. Legrand, Philos. Mag. A **59**, 321 (1989).
[13] M. S. Daw, in *Atomistic Simulation of Materials Beyond Pair Potential*, edited by V. Vitek and D. J. Srolovitz (Plenum, New York, 1989), p. 181.
[14] M. J. Stott and E. Zaremba, Solid State Commun. **32**, 1297 (1979).
[15] M. J. Stott and E. Zaremba, Phys. Rev. B **22**, 1564 (1980).
[16] M. J. Puska, R. M. Nieminen, and M. Manninen, Phys. Rev. B **29**, 3037 (1981).
[17] A. Banerjea and J. R. Smith, Phys. Rev. B **37**, 6632 (1988).
[18] K. W. Jacobsen, J. K. Norskvo, and M. J. Puska, Phys. Rev. B **35**, 7423 (1987).
[19] M. S. Daw, Phys. Rev. B **39**, 7441 (1989).
[20] J. A. Nelder and R. Mead, Comput. J. **7**, 308 (1965).
[21] R. A. Johnson, J. Mater. Res. **7**, 883 (1992).
[22] H. L. Skriver, Phys. Rev. B **31**, 1909 (1985).

[23] J. Neugebauer and M. Scheffler, Phys. Rev. B **46**, 16 067 (1992).
[24] H. M. Polatoglou, M. Methfessel, and M. Scheffler, Phys. Rev. B **48**, 1877 (1993).
[25] H. L. Skriver and N. M. Rosengaard, Phys. Rev. B **46**, 7157 (1992).
[26] F. R. de Boer, R. Boom, W. C. M. Mattens, A. R. Miedema, and A. K. Niessen, *Cohesion in Metals* (North-Holland, Amsterdam, 1988).
[27] T. Ning, Q. L. Yu, and Y. Y. Ye, Surf. Sci. Lett. **206**, L857 (1988).
[28] A. M. Guellil and J. B. Adams, J. Mater. Res. **7**, 639 (1992).
[29] R. Hultgren, P. D. Desai, D. T. Hawkins, M. Gleiser, and K. K. Kelley, *Selected Values of Thermodynamic Properties of Binary Alloys* (American Society for Metals Park, Metal Park, OH, 1973).
[30] A. R. Miedema, P. F. de Chatel, and F. R. de Boer, Physica **100B**, 1 (1980).
[31] K. Terakura, T. Oguchi, T. Mohri, and K. Watanabe, Phys. Rev. B **35**, 2169 (1987).
[32] S. Takizawa and K. Terakura, Phys. Rev. B **41**, 9717 (1989).
[33] *Handbook of Chemistry and Physics*, edited by R. C. Weast (CRC, Boca Raton, FL, 1984).
[34] J. S. Koehler, in *Vacancies and Interstitials in Metals*, edited by A. Seeger, D. Schumacher, W. Schilling, and J. Diehl (North-Holland, Amsterdam, 1970), p. 175.
[35] C. Kittel, *Introduction to Solid State Physics*, 5th ed. (Wiley, New York, 1976).
[36] *Metal Reference Book*, 5th ed., edited by C. J. Smith (Butterworths, London, 1976), p. 186.
[37] G. Simmons and H. Wang, *Single Crystal Elastic Constants and Calculated Aggregate Properties: A Handbook* (MIT Press, Cambridge, MA, 1971).
[38] R. W. Balluffi, J. Nucl. Mater. **69&70**, 240 (1978).
[39] W. Wycisk and M. Feller-Knipmeier, J. Nucl. Mater. **69&70**, 616 (1978).
[40] Y. A. Kraftmakher and P. G. Strelkov, in *Vacancies and Interstitials in Metals* (Ref. 34), p. 59.
[41] A. Seeger and H. Mehrer, in *Vacancies and Interstitials in Metals* (Ref. 34), p. 1.
[42] J. S. Koeher, in *Vacancies and Interstitials in Metals* (Ref. 34), p. 169.
[43] H. Kronmuller, in *Vacancies and Interstitials in Metals* (Ref. 34), p. 183.
[44] J. R. Noonan and H. L. Davis, Bull. Am. Phys. Soc. **26**, 224 (1981).
[45] R. J. Culbertson, L. C. Feldman, P. J. Silerman, and H. Boehn, Phys. Rev. Lett. **47**, 657 (1981).
[46] M. A. Van Hove, and S. Y. Tong, *Crystallography by LEED* (Springer, Berlin, 1979).
[47] H. L. Davis and J. R. Noonan, Surf. Sci. **126**, 245 (1983).
[48] D. L. Adams, H. B. Nielsen, and J. N. Andersen, Surf. Sci. **128**, 294 (1983).
[49] S. A. Lindgren, L. Wallden, J. Rundgren, and P. Westrin, Phys. Rev. B **29**, 567 (1984).
[50] J. W. M. Frenken, R. G. Smeenk, and J. F. Van der Veen, Surf. Sci. **135**, 147 (1983).
[51] D. L. Adams, L. E. Petersen, and C. S. Sorensen, J. Phys. C **18**, 1753 (1985).
[52] C. J. Ding, M. Lindroos, R. D. Diehl, and D. A. King, Surf. Sci. **162**, 59 (1985).
[53] J. A. Davis, T. E. Jackman, D. P. Jackson, and P. R. Norton, Surf. Sci. **109**, 20 (1981).
[54] J. A. Davis, D. P. Jackson, P. R. Norton, D. E. Posner, and W. N. Unertl, Solid State Commun. **34**, 41 (1980).